




RESEARCH ARTICLE | NOVEMBER 02 2023

Self-configuring programmable silicon photonic filter for integrated microwave photonic processors

C. Catalá-Lahoz ; D. Pérez-López ; T. Huy-Ho; J. Capmany 




APL Photonics 8, 116103 (2023)

<https://doi.org/10.1063/5.0169544>




CrossMark



yttrium iron garnet, zeolites, nano ribbons, epitaxial crystal growth, cerium oxide polishing powder, surface functionalized nanoparticles, refractory metals, laser crystals, anodic aluminum oxide, niobate, InAs wafers, ZnS, CdTe, perovskite crystals, transparent ceramics

glassy carbon, III-IV semiconductors, barium fluoride, europium phosphors, ultra high purity materials, cermet, nanodispersions, MBE grade materials, thin film, OLED lighting, solar energy, sputtering targets, fiber optics, h-BN, deposition slugs, CVD precursors, photovoltaics, metamaterials, borosilicate glass, YBCO superconductors, InGaAs, indium tin oxide, MgF2, rutile, diamond micropowder, optical glass

beamsplitters, fused quartz, additive manufacturing, organometallics, infrared dyes, transparent ceramics, CIGS, cermet, nanodispersions, MBE grade materials, thin film, OLED lighting, solar energy, sputtering targets, fiber optics, h-BN, deposition slugs, CVD precursors, photovoltaics, metamaterials, borosilicate glass, YBCO superconductors, InGaAs, indium tin oxide, MgF2, rutile, diamond micropowder, optical glass



Now Invent.™

www.americanelements.com

© 2001-2022, American Elements LLC, a U.S. Registered Trademark

The Next Generation of Material Science Catalogs

Self-configuring programmable silicon photonic filter for integrated microwave photonic processors

Cite as: APL Photon. 8, 116103 (2023); doi: 10.1063/5.0169544
Submitted: 26 July 2023 • Accepted: 15 October 2023 •
Published Online: 2 November 2023



View Online



Export Citation



CrossMark

C. Catalá-Lahoz,^{1,a)}  D. Pérez-López,²  T. Huy-Ho,³ and J. Capmany^{1,b)} 

AFFILIATIONS

¹ Photonics Research Labs, iTEAM Research Institute, Universitat Politècnica de València, Valencia, Spain

² iPronics Programmable Photonics S.L., Valencia, Spain

³ Ottawa Wireless Advanced System Competency Centre, Huawei Technologies Canada Co., Ltd., Ottawa, Ontario L3R 5A4, Canada

^{a)} Author to whom correspondence should be addressed: ccatala@iteam.upv.es

^{b)} E-mail: jcapmany@iteam.upv.es

ABSTRACT

Reconfigurable photonic filters show great promise as a potential solution to meet the evolving needs of future microwave communication systems. By integrating high-performance filters into programmable microwave photonic processors, they can provide significant benefits for signal processing applications. The development of an algorithm that can automatically characterize and reconfigure the filter using a single optical input and output port is essential for this purpose. This paper presents an optimization technique for a fully tunable ring-assisted Mach–Zehnder interferometer filter. The proposed filter design eliminates the need for monitoring components and employs a novel algorithm that operates independently in each ring by switching between the two arms of the filter. In addition, the filter can be configured to implement different filter architectures, allowing for flexible filtering requirements. Measurements were performed using the device as an interleaver, implementing different types of infinite impulse response filters in the optical and radio frequency domains. Side-coupled integrated spaced sequence of resonator filters were also implemented by reconfiguring the same device. These results demonstrate the exceptional reconfigurability of the filter design proposed herein in terms of bandwidth and central frequency.

© 2023 Author(s). All article content, except where otherwise noted, is licensed under a Creative Commons Attribution (CC BY) license (<http://creativecommons.org/licenses/by/4.0/>). <https://doi.org/10.1063/5.0169544>

I. INTRODUCTION

Programmable photonic integrated circuits (PICs)^{1–4} stand out as a prominent alternative within the domain of integrated microwave photonic (IMWP) processors.^{5,6} The integration of reconfigurable optical cores, alongside modulation and photodetection subsystems, empowers the development of comprehensive tunable photonic devices. With these, we can effectively address the dynamic demands of wideband spectral processing in a wide variety of emerging application scenarios, such as flexible transceivers and multiplexers in high-speed fiber communications,⁷ and also for the implementation of upgradable interfaces for future communication systems.^{8,9} Furthermore, these features are key to high-speed reconfigurable interconnections in computing systems as well as the realization of quantum logic gates.^{10–13} Moreover, their

implementation in a silicon photonic platform offers advantages, such as compatibility with existing CMOS fabrication processes, compact footprint, and low power consumption.

Among the large gamut of applications for IMWP processors, RF photonic signal filtering stands out as one of the most prevalent and widely adopted functionalities.^{14–19} IMWP filters offer a remarkable ability to achieve ultra-wideband frequency tunability, providing a practical solution to the limitations commonly encountered with conventional electronic filters. RAMZI (Ring-Assisted Mach–Zehnder Interferometer) filters are an outstanding option due to their high-resolution spectral filtering and on-chip spectral processing capabilities.^{20–27} This filter structure benefits from the advantages of all-pass filters to achieve arbitrary bandpass filters,²⁸ combining both FIR (Finite Impulse Response) and IIR (Infinite Impulse Response) filters. The integration of various filter types into

a single device with programmable and reconfigurable capabilities makes it ideal for an extensive range of applications in optical signal processing and RF filtering.

The use of monitors to characterize and optimize RAMZI filters is a recently reported effective strategy.^{29,30} However, the implementation of this approach in a field programmable photonic gate array (FPGA) poses challenges.³¹ Accessing each of the rings from different ports in a mesh architecture results in increased power losses and an inefficient utilization of the device, wasting a significant part of the optical ports. In addition, the final packaging of the device becomes more complex due to the requirement of analog-to-digital converters (ADCs) and transimpedance amplifiers (TIAs) at the output of the photodetectors.

Here, we propose an optimization technique for a multipurpose RAMZI filter, and we demonstrate it with a fully tunable design of such a kind of filters, which only requires a single input and a single output optical port for both characterization and tuning processes and may dispense with an electrical monitoring system. By eliminating the need for additional monitoring components, our technique also circumvents the losses induced by the couplers required for that purpose. Moreover, the proposed filter is capable of implementing different architectures. By incorporating tunable couplers at the input and at the output, the filter arms can be selectively activated, enabling the structure to operate as an independent notch filter or as a Side-Coupled Integrated Spaced Sequence of Resonators (SCISSOR)-type RF filter³² with an improved spectral selectivity. These results are experimentally assessed by means of a fourth-order RAMZI filter, fabricated using silicon-on-insulator technology. Along this line, an auto-characterization algorithm has been developed to know each ring coupling curve. Subsequently, different types of filters have been configured, demonstrating their reconfiguration capabilities in bandwidth and central frequency. Bandpass filters with bandwidths ranging from 5 to 40 GHz are implemented and measured, tuning their central frequency from 0 to 50 GHz in both optical and RF domains. Furthermore, we demonstrate its operation as a SCISSOR filter using different types of modulation to achieve bandpass and band-stop filters, as well as its reconfigurability.

II. FILTER DESIGN

In the response of a digital filter, the design parameters are defined by its poles and zeros. From these parameters, we can synthesize different spectral responses in integrated photonic structures. Using an interferometric structure, we need to decompose the response of the designed digital filter into the sum of two all-pass functions. A simplified RAMZI filter is based on the use of a cascade of rings on each arm of the Mach-Zehnder Interferometer (MZI), thus implementing the two all-pass functions on each arm.³³ The total number of rings used gives the order of the filter, as each ring implements a pole-zero pair. Since this type of filter has the versatility of using programmable unit cells throughout the structure, we can create multiple types of filters and arbitrary responses by programming them. Figure 1 shows the proposed design for a general simplified RAMZI structure of order N .

Each ring contains an MZI coupler to tune its coupling (κ_n) and a phase shifter to tune its resonance (ϕ_n). In addition, MZI couplers have also been added to the input and output of the filter

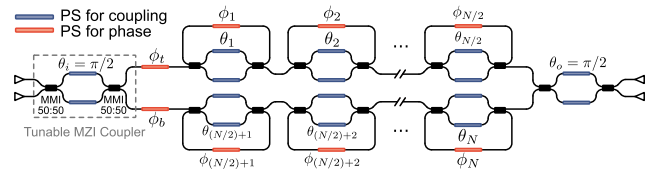


FIG. 1. N th-order cascade ring implemented filter with input and output tunable MZIs and tunable rings.

(θ_i and θ_o), allowing switching between the upper and lower arms. This allows for full characterization of the rings separately and additional filter architectures, such as SCISSOR or notch filters. Finally, the top and bottom phase shifters (ϕ_t and ϕ_b) are added in the two arms to tune the out-of-band rejection of the filter. The transfer function of a tunable ring in the Z -domain is as follows:

$$H_r(z) = -e^{j\Delta} \frac{j \sin(\theta/2) + \alpha e^{j(\Delta+\phi)} z^{-1}}{1 - j\alpha \sin(\theta/2) e^{j(\Delta+\phi)} z^{-1}}, \quad (1)$$

where $\theta = \phi_u - \phi_d$ and $\Delta = (\phi_u + \phi_d)/2$, with ϕ_u and ϕ_d being the two phase shifters of each MZI, and α is the round trip loss of the ring. The transfer functions of the upper and lower arms, respectively, are the product of the ring transfer functions multiplied by the phase shift of each arm,

$$A_1(z) = e^{j\phi_t} \prod_{k=1}^{N/2} H_{r_k}(z), \quad (2)$$

$$A_2(z) = e^{j\phi_b} \prod_{k=N/2}^N H_{r_k}(z). \quad (3)$$

To obtain the couplings and phases of the RAMZI elements, we calculate the poles of $A_1(z)$ and $A_2(z)$, extracting the roots of their denominators. We then perform a translation of the poles to the optical domain by multiplying the roots r by the normalized central frequency,

$$r_{\omega_0} = r e^{j(\omega_0/\text{FSR}_{\text{Hz}})}, \quad (4)$$

where ω_0 is the desired optical central frequency of the filter and FSR_{Hz} is the Free Spectral Range (FSR) of the rings in hertz. Knowing that each ring implements a pole, we can obtain the coupling and phase parameters from the transfer function denominator of the ring,

$$p_n = \frac{e^{-j(\Delta_n+\phi_n)}}{j\alpha \sin(\theta_n/2)}, \quad (5)$$

where p_n are the pole values of the two all-pass functions obtained from the decomposition algorithm. From the module and phase values of each pole, we extract the coupling and phase parameters of each ring, θ_n and ϕ_n , respectively. Finally, from this algorithm, a parameter β is obtained, which corresponds to the phase applied to each arm of the filter. In an even order filter, due to its symmetry, the values of each front phase shifter are $\phi_t = \beta$ and $\phi_b = -\beta$. In practice,

it is not necessary to tune the two phase shifters, only that the difference between the two arms of the filter is the same (e.g., $\phi_t = 2\beta$ and $\phi_b = 0$).

By employing the algorithm within a RAMZI-like structure utilizing all-pass filters, it becomes feasible to construct arbitrary bandpass filters by combining FIR and IIR filters. Although lattice-type structures have been suggested for this purpose, they need a greater number of tunable couplers and phase shifters compared to filters of the same order. Alternatively, by equipping the filter with tunable couplers at the input and output, each arm of the filter can be used independently. This flexibility allows us to configure the rings separately, enabling them to be used as notch filters for processing or to create SCISSOR-type RF filters with narrower bandwidths.

III. FABRICATED DEVICE

To showcase the capabilities of the filter, we have successfully fabricated a fourth-order RAMZI filter using silicon-on-insulator (SOI) technology. The fabrication process involved 193-nm deep ultraviolet (DUV) lithography at the AMF SiP foundry. Figure 2 shows a detailed photograph of the fabricated device, highlighting a tunable ring. The overall structure of the filter, which includes pad arrays for electrical signals, measures 2980×1170 m. Strip waveguides with a height of 220 nm and a silicon core width of 500 nm are employed, whose propagation losses are 1 dB/cm. For the input

and output ports of the filter, we have used 1D grating couplers, with insertion losses of around 5 dB/facet. The measured effective index value of this platform is around 2.38–2.41.

The tunable rings are designed with a tunable MZI consisting of 2×2 multimode interferometers (MMIs) and phase shifters to enable precise tuning of the ring's coupling and resonance wavelength. MMI-based tunable couplers have higher insertion losses (0.5–0.7 dB) compared to a plain dual-drive directional coupler (0.2 dB), but the former enjoy broader bandwidth operation (>40 nm) compared to DC-based ones (around 10 nm).³⁴ The chip contains a total of 12 MMIs and 18 phase shifters, of which only 11 are driven, one of each tunable MZI and one of the two front phase shifters. The power consumption per π phase shift for each phase shifter is ~ 1.3 mW. Hence, in the worst case, the device would consume at most 14.3 mW, which means a very low power consumption. The round trip length of the ring is set to $1310 \mu\text{m}$, resulting in a 55 GHz FSR and a Q-factor of $2.28 \cdot 10^5$. In place of simple directional couplers, tunable MZIs are also used at the input and output of the RAMZI structure, allowing for switching between the upper and lower arms. This configuration facilitates independent characterization and tuning of each ring without the need for monitoring, greatly simplifying the overall device. Moreover, it provides versatility in achieving different types of filters. For instance, by putting the input and output MZIs in the bar state, we can create a second-order side-coupled integrated spaced sequence of resonators (SCISSOR) filter. Alternatively, employing only one ring enables the creation of a single notch filter.

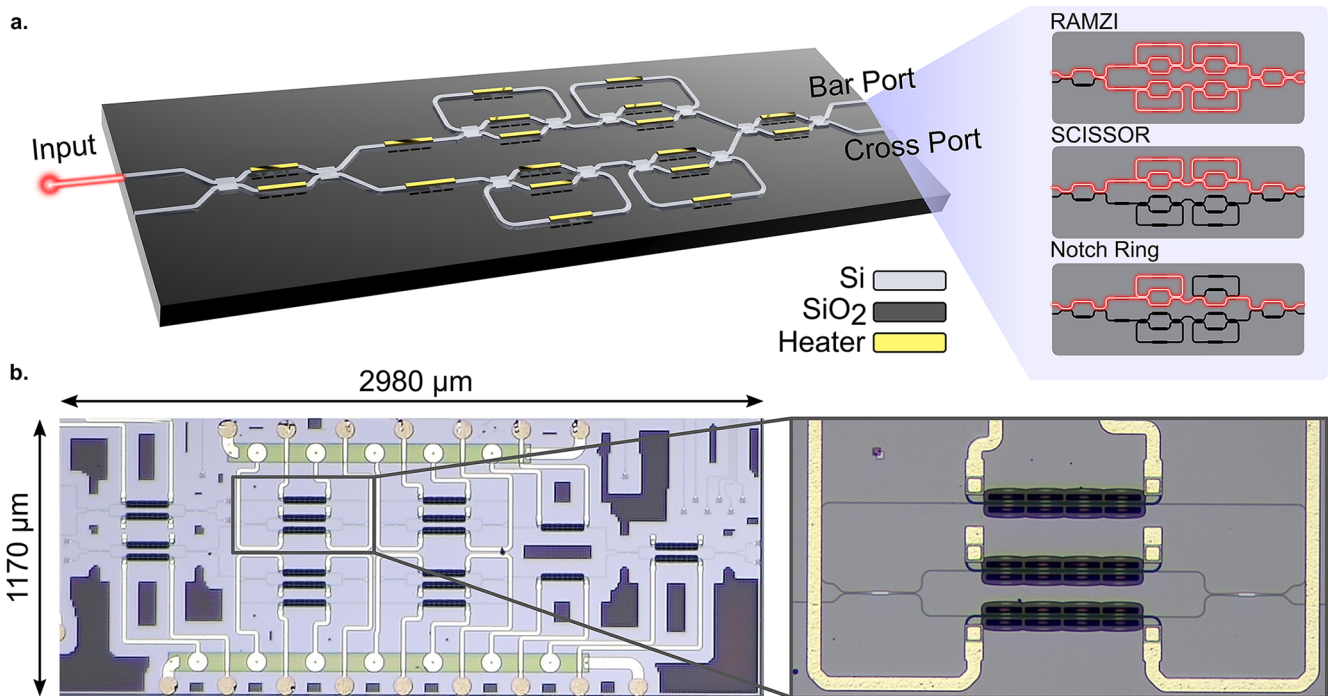


FIG. 2. Concept of the fabricated programmable photonic filter. (a) Fourth-order filter device design and examples of different implementations for the output circuit. (b) Micrograph of the fabricated chip with details of one tunable ring.

Throughout the entire structure, we incorporate thermo-optical phase shifters, which work in conjunction with trenches to avoid thermal crosstalk and achieve lower power consumption.

IV. DEVICE CHARACTERIZATION AND TUNING ALGORITHMS

Tuning of the photonic filters is accomplished by precisely adjusting the resonance of each ring independently. To achieve this, it is necessary to characterize the coupling factor of each ring individually. In addition, since we have tunable MZIs at both the input and output of the filter, it is essential to characterize them as well in order to facilitate switching between the upper and lower arms to access the individual response of each ring. The block diagram in Fig. 3(a) shows the algorithm used for the characterization of these two components, separating it into two parts: first, the characterization of the input and output MZIs, and second, the characterization of the rings.

To characterize the input and output MZIs, a fixed-wavelength laser is utilized at the input of the filter. For each MZI, specific current values are set for one of the phase shifters. The optical output power of the filter at the bar port is then measured for all the different combinations of these current values, as depicted in Fig. 3(b). The minimum received power values correspond to totally opposite states (bar or cross) at the input and output MZIs, e.g., $\kappa_i = 0$ and $\kappa_o = 1$. This indicates that all the power is directed to the cross port of the filter.

By extracting the power curves for the remaining current values at these specific points, we obtain the output power curve as a function of the current set for one of the MZIs. In this configuration, the other MZIs are programmed to operate as a waveguide rather than an interferometer, enabling independent measurement. Normalizing the output power measurements, we can derive the transmission factor at the bar port, denoted as $t_{\text{bar}} = \sin^2(\theta/2)$.

In an ideal MZI, the initial state with no applied current would correspond to the cross state. However, due to fabrication variations, we may encounter deviations in the initial phase θ . To account for this, we can fit the programmed phase relative to the current I using the following equation:

$$\theta = p_1 I^2 + p_0, \tag{6}$$

where p_0 and p_1 are the fitting parameters. Figure 3(c) represents the obtained coupling factor and phase from characterized input and output MZIs.

For characterizing the rings, we employ a tunable laser to measure the transfer function of each ring by switching between the upper and lower arms of the structure and decoupling the rest of the rings. The result of sweeping the current in the coupling phase shifter of the MZI is shown in Fig. 3(d). From the Extinction Ratio (ER) of the resonance for each current, we can determine the transmission factor from the following relationship:

$$\text{ER} = \frac{(\alpha + t)^2 (1 - \alpha t)^2}{(t - \alpha)^2 (1 + \alpha t)^2}. \tag{7}$$

Figure 3(e) shows the coupling factor and phase obtained for four different rings.

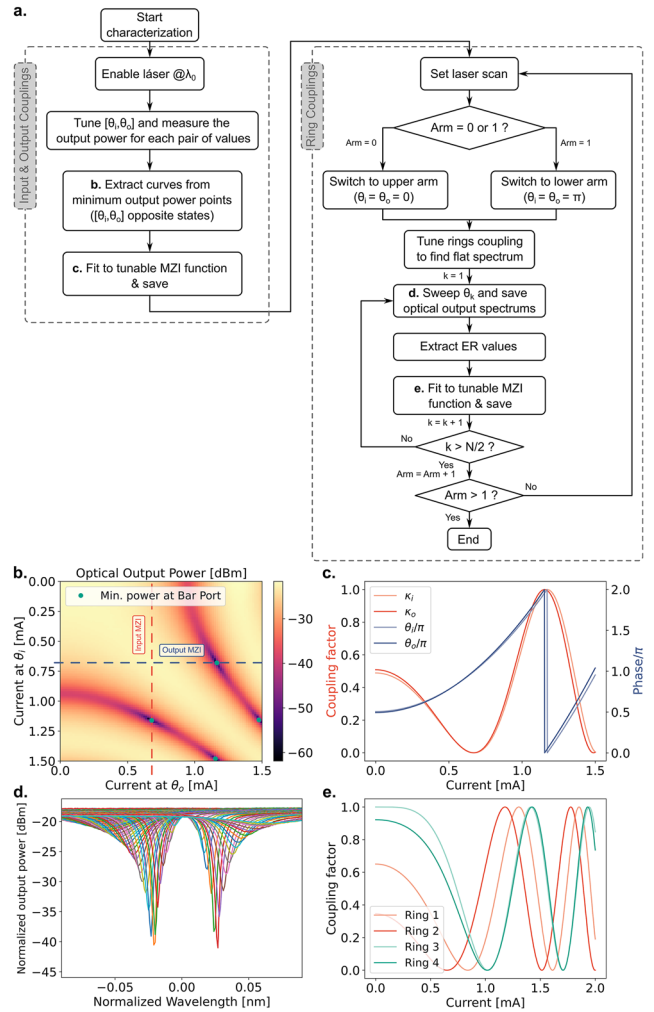


FIG. 3. (a) Characterization algorithm for a N th-order RAMZI filter architecture. (b) Optical output power curves for different input and output couplings. (c) Characterized input and output couplings and phase. (d) Optical spectrum of a tunable ring for different couplings. (e) Characterized ring couplings.

After fully characterizing the device, tuning is performed for the desired filter response. Figure 4(a) represents the followed procedure to set a filter with the obtained parameters from (5). The rings of the upper arm are set to a $\kappa = 0$ coupling to achieve a flat frequency response. Each ring is then separately tuned to the desired θ value using the characterization curves of Fig. 4(c). The extinction ratio of the resonance is optimized to match the simulated response of the ring, that changes the magnitude of the pole position. The ring phase is tuned by increasing the current in the corresponding phase shifter heater, causing a resonance shift in wavelength, which changes the angle of the pole position. Using a laser fixed at the desired resonance wavelength, the output optical power of the filter is measured until finding a power minimum. The current values for θ and ϕ of each ring are optimized in the same way for the remaining

rings. Finally, the input and output couplings are set to $\kappa_i = \kappa_o = 0.5$, and one of the front phase shifters is tuned by increasing its current to find the final response of the filter by comparing the measured response with the simulated response. The minimum MSE provides the final response of the optimized filter. An optimization algorithm with progressive refinement is used to optimize each of the currents, both in the coupling and phase of the rings and in the front phase shifter. In this way, we can effectively find the optimal current value with sufficient resolution. This tuning method remains effective when operating within a band around the wavelength used for device characterization, since the MZI coupling factor is wavelength dependent.

Figure 4(b) shows the pole and zero diagram of a Chebyshev type II filter designed with a bandwidth of 20 GHz (36% of the FSR) and a stopband attenuation of 30 dB. Below, the table of parameters obtained from the decomposition algorithm is provided. In Fig. 4(c), we can see the simulated response of the filter in frequency together with the corresponding response that each ring has separately.

Both the characterization and tuning algorithms have been implemented in Python, together with the control of the instrumentation used, as well as the complete polynomial decomposition algorithm with which the filter parameters are obtained. Consequently, the script only requires the input parameters specifying

the desired characteristics of the digital filter. The set of algorithms within the script takes care of the rest, streamlining the implementation process.

V. EXPERIMENTAL RESULTS

A. Fourth-order simplified RAMZI filter

The characterization of the device, as well as the tuning of the different types of filters, was carried out by measuring the spectrum in wavelength. The PIC is placed on a thermoelectric cooler (TEC) with thermal grease paste, which is responsible for keeping the temperature of the device stable, together with a heat sink to dissipate the heat. Keeping the temperature stable during the execution of the calibration and tuning algorithms is crucial to preventing the ring resonances from drifting. Cleaved fibers have been used to enter and exit the chip through grating couplers.

To measure the optical spectrum, we have used a tunable laser together with a component tester (EXFO T100S-HP and CT440), both controlled through a Python script. To feed the electrical signals, we have used multi-channel voltage sources (Qontrol Ltd.), also controlled by the same script, which are connected to multi-contact probes (MPI TITAN™) with which we make contact directly with the chip pads.

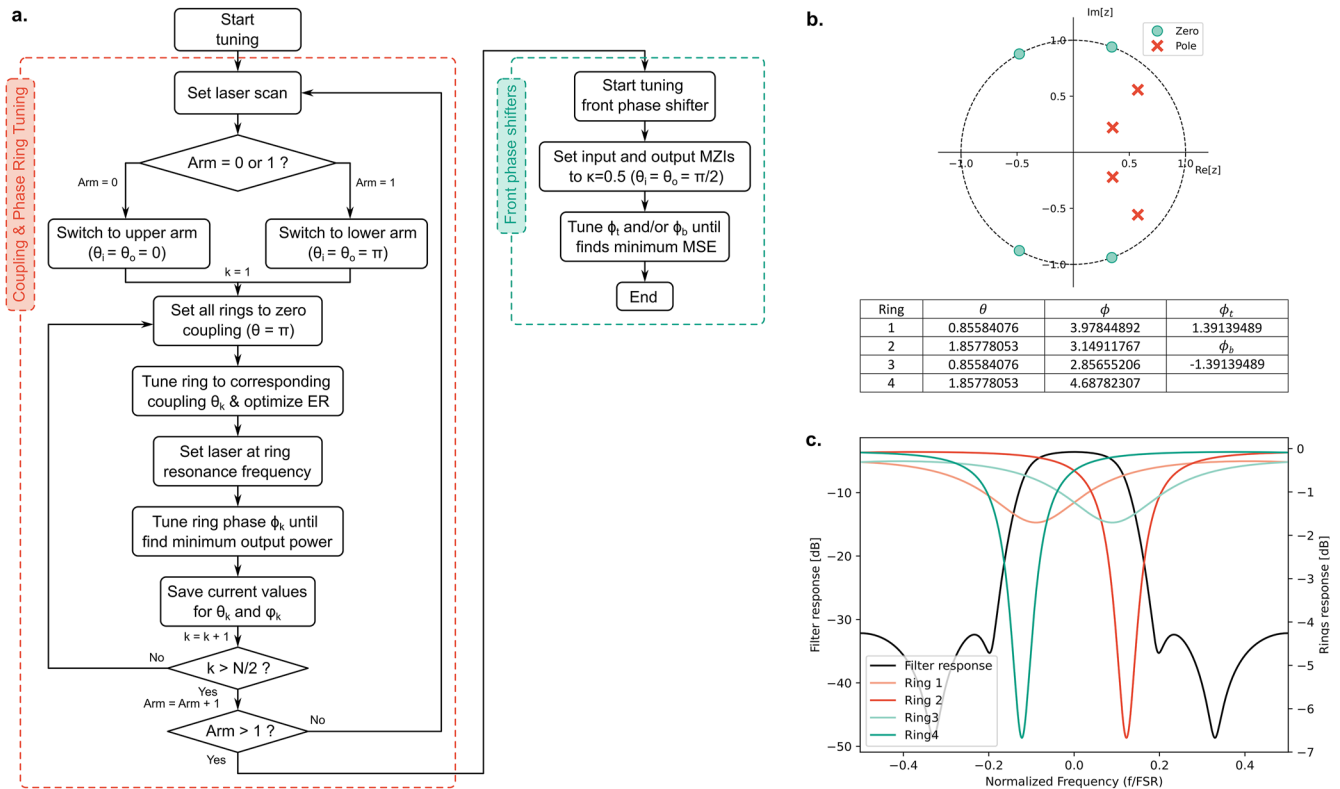


FIG. 4. (a) Tuning algorithm for an *N*th-order RAMZI filter. (b) Example of a pole/zero diagram and parameters for a Chebyshev type II filter with 20 GHz bandwidth and 30 dB stopband attenuation. (c) Chebyshev type II filter response example with the corresponding response of each ring.

Due to the inherent reconfigurability of the filter, a diverse range of designs can be implemented. This flexibility allows for the construction of IIR filters, such as Butterworth, elliptic, and Chebyshev of up to fourth order, contingent upon the number of rings employed. By leveraging the addition or subtraction of two all-pass functions, these filter types can be realized effectively. Notably, when both output ports of the filter are utilized, complementary responses are obtained, thereby enabling the device to function as an interleaver.

Figure 5 presents the experimental measurements of four distinct types of IIR filters, with different bandwidths. For all filter types, the optimization process employed the tuning algorithm discussed in Sec. IV. Notably, the measured responses fit perfectly with their corresponding simulated responses, considering the losses induced by the rings. Note that the frequency input to the Chebyshev type II design function sets the beginning of the stopband rather than the end of the passband as in the other designs.

The configuration parameters acquired during the calibration process for each filter can be preserved and utilized subsequently, as long as the temperature remains the same. It is important to note that alterations in temperature do not impact the shape of the filter; however, they do affect its center frequency.

The filters exhibit complete reconfigurability, allowing for adjustments in both the center frequency and bandwidth to cater to diverse applications. Figure 6 demonstrates the reconfiguration of the center frequency across the entire FSR. In an ideal scenario, this reconfiguration could be achieved by uniformly shifting the phase of all four rings. However, due to variations in the group index with wavelength and certain thermal crosstalk between rings, large frequency displacements are not feasible. Consequently, a partial tuning algorithm is necessary to move the resonances to the corresponding wavelengths at the four rings.

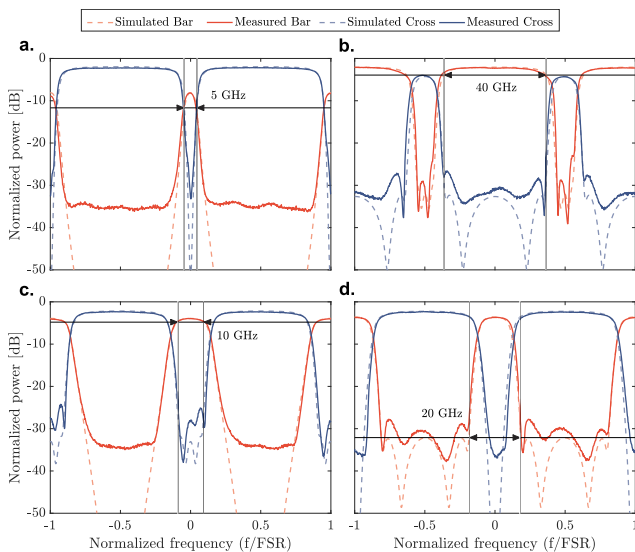


FIG. 5. Measured fourth-order filters in bar and cross ports: (a) Butterworth filter with 5 GHz bandwidth in bar port, (b) elliptic filter with 40 GHz bandwidth in bar port, (c) Chebyshev type I filter with 10 GHz bandwidth in bar port, and (d) Chebyshev type II filter with 20 GHz bandwidth in bar port.

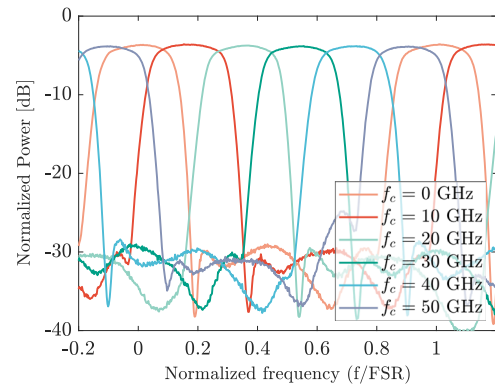


FIG. 6. Reconfiguration of a fourth-order elliptic filter with 10 GHz bandwidth at six different frequencies in the full FSR spectrum.

For bandwidth reconfiguration, the entire algorithm must be rerun, as both the amplitude and phase of the poles and zeros change completely compared to other bandwidths. Figure 7 shows the remarkable reconfigurability capacity of four distinct filter types, spanning bandwidths ranging from 5 to 40 GHz while maintaining a stopband attenuation of 30 dB. It is important to note that the passband losses increase as the bandwidth decreases due to ring round trip losses. Among the various filters, Butterworth and Chebyshev type II filters exhibit wider transition bands, while Chebyshev type I and elliptic filters demonstrate a faster roll-off. For example, the slope rate obtained for the elliptical and Chebyshev type I filters is 7.66 and 6 dB/GHz, respectively, in the filters measured with

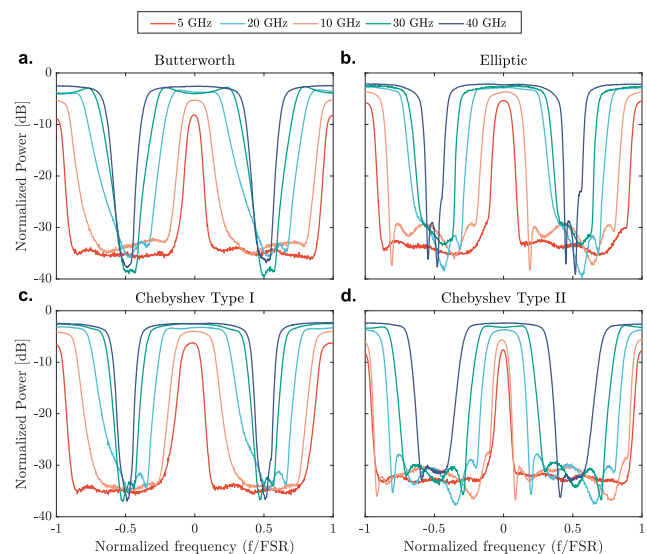


FIG. 7. Measured fourth-order filters in the bar port performing bandwidth reconfiguration for (a) Butterworth filter, (b) elliptic filter, (c) Chebyshev type I filter, and (d) Chebyshev type II filter.

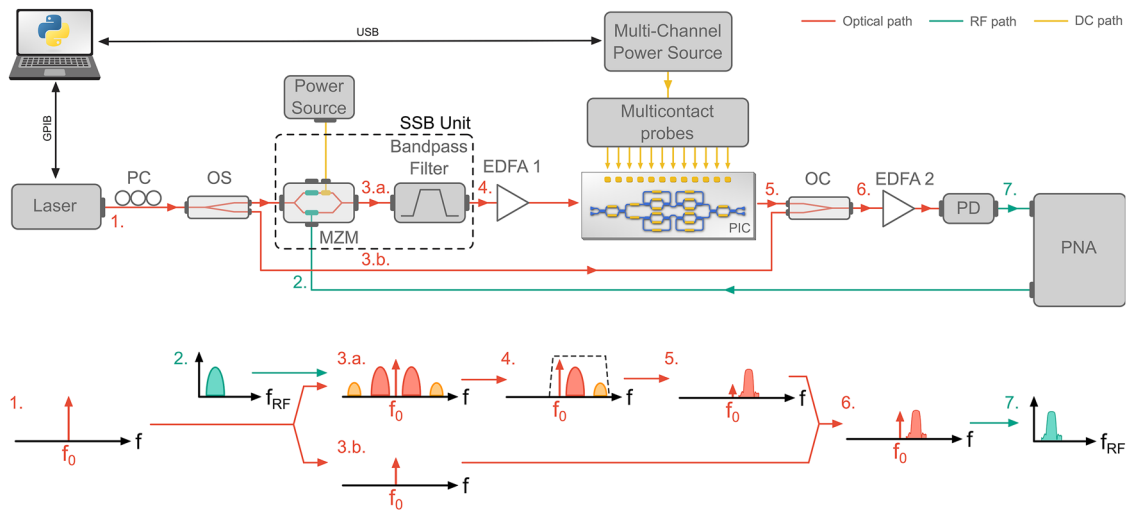


FIG. 8. Setup configuration for radio frequency measurements of the RAMZI filter using carrier re-injection and optical/RF signal flow.

40 GHz bandwidth. Meanwhile, for the Chebyshev type II and Butterworth filters, we obtained a slope rate of 4.95 and 4.42 dB/GHz, respectively.

To demonstrate the tunable microwave photonic (MWP) filter, single-sideband (SSB) modulation is employed. In this setup, we utilize a dual-drive intensity modulator (DD-MZM Sumitomo T.DEH1.5-40-ADC) in conjunction with a wave-shaper incorporating a stopband filter to eliminate one of the RF sidebands. A schematic diagram illustrating the microwave photonic system experiment is presented in Fig. 8.

Initially, an optical carrier generated by a laser source is split into two paths using a 90/10 optical splitter (OS). The 10% fraction is directed to the external part of the photonic integrated circuit (PIC), while the remaining 90% is subjected to modulation. The dual-drive MZM is modulated using a performance network analyzer (PNA), operating at the optimum quadrature bias (QB) point. The SSB-modulated signal is then amplified by an erbium-doped fiber amplifier (EDFA) before being coupled into the optical integrated filter via a cleaved fiber. Subsequently, the filtered signal is collected at the filter output using another cleaved fiber. Once outside the chip, the carrier is recombined with the signal using a 50/50 optical coupler (OC). Finally, the complete signal is further amplified by an additional EDFA before being sent to a photodetector and the network analyzer. Figure 9 displays the measurements obtained from an elliptical filter, demonstrating its tunability at five different frequencies. In this case, the frequency tuning was achieved by shifting the phase of the rings as shown in Fig. 6.

B. Second-order SCISSOR filter

The circuit’s total reconfigurability enables us to achieve a versatile setup. By configuring the input and output MZIs in the bar state, we can effectively establish two distinct SCISSOR filters on each output port. These specialized filters offer significant advantages, such as narrower bandwidths, making them highly valuable in communication applications.

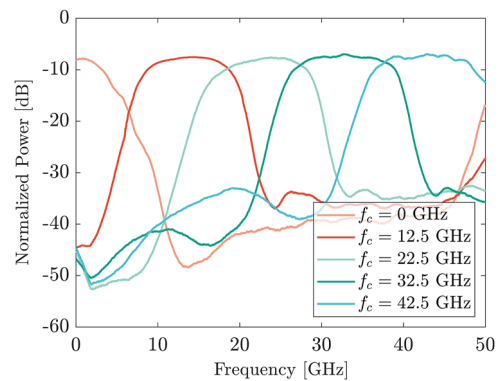


FIG. 9. Measured fourth-order elliptical filter with 10 GHz bandwidth at five different frequencies in the radio frequency domain.

For its demonstration, the above structure has been configured to implement bandpass and band-stop filters in the RF domain. A modulated optical signal passes through the upper or lower arm of the filter, which is composed of two cascade ring resonators. The RF signal is modulated to generate a double-sideband (DSB) spectrum. One of the ring resonances needs to be in the frequency range of the lower sideband, and the other needs to be in the frequency range of the upper sideband. The two rings must be in critical coupling, as that will result in a sharp slope phase response. By means of direct detection, the two processed sidebands are down-converted back into two RF components and interfere with each other. When the resonances of the two resonators are aligned at different frequencies of the sidebands, the equivalent RF responses have a region with a phase difference of π .

Using an intensity modulator (such as a quadrature-biased MZM) produces two sidebands that are in phase with the carrier, while a phase modulator generates sidebands with a complementary

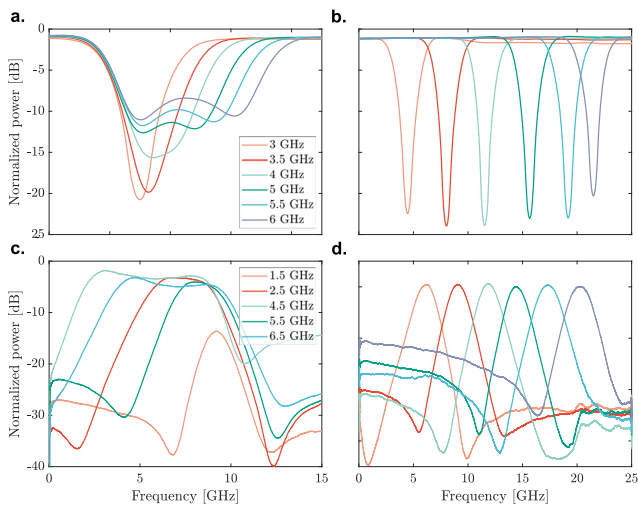


FIG. 10. Measured SCISSOR filter: (a) band-stop response tuning bandwidth and (b) tuning central frequency; (c) bandpass response tuning bandwidth and (d) tuning central frequency.

phase relation. This particular frequency region will be translated into a rejection band in the case of intensity modulation or into a transmission band in the case of a phase modulation. Figure 10 shows the experimental results using the two types of modulation and demonstrates the bandwidth and center frequency tuning capability, being able to obtain filters from 1.5 GHz of bandwidth centered at 20 GHz or more.

VI. CONCLUSION

In this work, we demonstrate a high-performance photonic filter that can be reconfigured automatically. The algorithm can adaptively tune the filter rings to achieve reconfiguration of bandwidth and central frequency. The programmability and scalability of these filters make them promising for a variety of applications, such as fully integrated RF photonic front-ends, beamforming, and image processing, due to their need for a rapid change in real-world scenarios.

Moreover, the proposed design brings the possibility of its incorporation into photonic processors since it is not necessary to use monitors for the calibration and tuning procedures. Embedding alternatives are used as a high-performance building block (HPBB) or for programming its structure within a mesh. The latter would require very short programmable unit cells (PUCs) to achieve rings with a short round trip length and a large FSR. Higher-order IIR filters can be implemented for better performance on lower bandwidth filters, adding more rings to the design. Higher Q-factor in the rings, which reduces their losses as well as their length, is an improvement to consider for future designs, achieving higher order filters with low losses and a higher FSR.

ACKNOWLEDGMENTS

We acknowledge the financial support by Huawei through Contract No. YB20200065124 and the Generalitat Valenciana Project No. PROMETEO/2021/015.

AUTHOR DECLARATIONS

Conflict of Interest

The authors have no conflicts to disclose.

Author Contributions

C. Catalá-Lahoz: Conceptualization (equal); Data curation (equal); Formal analysis (equal); Investigation (equal); Methodology (equal); Software (equal); Validation (equal); Visualization (equal); Writing – original draft (equal); Writing – review & editing (equal). **D. Pérez-López:** Conceptualization (equal); Data curation (equal); Formal analysis (equal); Supervision (equal); Writing – review & editing (equal). **T. Huy-Ho:** Conceptualization (equal); Project administration (equal); Supervision (equal). **J. Capmany:** Conceptualization (equal); Data curation (equal); Funding acquisition (equal); Project administration (equal); Supervision (equal); Validation (equal); Writing – review & editing (equal).

DATA AVAILABILITY

The data that support the findings of this study are available from the corresponding author upon reasonable request.

REFERENCES

- J. Capmany and D. Pérez, *Programmable Integrated Photonics* (Oxford University Press, 2019).
- J. C. Lyke, C. G. Christodoulou, G. A. Vera, and A. H. Edwards, "An introduction to reconfigurable systems," *Proc. IEEE* **103**, 291–317 (2015).
- W. Bogaerts, D. Pérez, J. Capmany, D. A. B. Miller, J. Poon, D. Englund, F. Morichetti, and A. Melloni, "Programmable photonic circuits," *Nature* **586**, 207–216 (2020).
- X. Xu, G. Ren, T. Feleppa, X. Liu, A. Boes, A. Mitchell, and A. J. Lowery, "Self-calibrating programmable photonic integrated circuits," *Nat. Photonics* **16**, 595–602 (2022).
- J. Capmany, I. Gasulla, and D. Pérez, "The programmable processor," *Nat. Photonics* **10**, 6–8 (2016).
- D. Pérez, I. Gasulla, L. Crudgington, D. J. Thomson, A. Z. Khokhar, K. Li, W. Cao, G. Z. Mashanovich, and J. Capmany, "Multipurpose silicon photonics signal processor core," *Nat. Commun.* **8**, 636 (2017).
- D. Melati, A. Alippi, A. Annoni, N. Peserico, and A. Melloni, "Integrated all-optical MIMO demultiplexer for mode- and wavelength-division-multiplexed transmission," *Opt. Lett.* **42**, 342 (2017).
- R. Waterhouse and D. Novack, "Realizing 5G: Microwave photonics for 5G mobile wireless systems," *IEEE Microwave Mag.* **16**, 84–92 (2015).
- W. Zhang, A. Tait, C. Huang, T. Ferreira de Lima, S. Bilodeau, E. C. Blow, A. Jha, B. J. Shastri, and P. Prucnal, "Broadband physical layer cognitive radio with an integrated photonic processor for blind source separation," *Nat. Commun.* **14**, 1107 (2023).
- A. Peruzzo, A. Laing, A. Politi, T. Rudolph, and J. L. O'Brien, "Multimode quantum interference of photons in multiport integrated devices," *Nat. Commun.* **2**, 224 (2011).
- B. J. Metcalf, N. Thomas-Peter, J. B. Spring, D. Kundys, M. A. Broome, P. C. Humphreys, X.-M. Jin, M. Barbieri, W. Steven Kolthammer, J. C. Gates, B. J. Smith, N. K. Langford, P. G. Smith, and I. A. Walmsley, "Multiphoton quantum interference in a multiport integrated photonic device," *Nat. Commun.* **4**, 1356 (2013).
- M. Zhang, L. Feng, M. Li, Y. Chen, L. Zhang, D. He, G. Guo, G. Guo, X. Ren, and D. Dai, "Supercompact photonic quantum logic gate on a silicon chip," *Phys. Rev. Lett.* **126**, 130501 (2021).

- ¹³S. Gyger, J. Zichi, L. Schweickert, A. W. Elshaari, S. Steinhauer, S. F. Covre da Silva, A. Rastelli, V. Zwiller, K. D. Jöns, and C. Errando-Herranz, "Reconfigurable photonics with on-chip single-photon detectors," *Nat. Commun.* **12**, 1408 (2021).
- ¹⁴J. S. Fandiño, P. Muñoz, D. Doménech, and J. Capmany, "A monolithic integrated photonic microwave filter," *Nat. Photonics* **11**, 124–129 (2017).
- ¹⁵Y. Xie, Z. Geng, L. Zhuang, M. Burla, C. Taddei, M. Hoekman, A. Leinse, C. G. Roeloffzen, K.-J. Boller, and A. J. Lowery, "Programmable optical processor chips: Toward photonic RF filters with DSP-level flexibility and MHz-band selectivity," *Nanophotonics* **7**, 421–454 (2017).
- ¹⁶W. Zhang and J. Yao, "On-chip silicon photonic integrated frequency-tunable bandpass microwave photonic filter," *Opt. Lett.* **43**, 3622 (2018).
- ¹⁷Y. Liu, A. Choudhary, D. Marpaung, and B. J. Eggleton, "Integrated microwave photonic filters," *Adv. Opt. Photonics* **12**, 485 (2020).
- ¹⁸Y. Tao, H. Shu, X. Wang, M. Jin, Z. Tao, F. Yang, J. Shi, and J. Qin, "Hybrid-integrated high-performance microwave photonic filter with switchable response," *Photonics Res.* **9**, 1569 (2021).
- ¹⁹O. Daulay, G. Liu, K. Ye, R. Botter, Y. Klaver, Q. Tan, H. Yu, M. Hoekman, E. Klein, C. Roeloffzen, Y. Liu, and D. Marpaung, "Ultrahigh dynamic range and low noise figure programmable integrated microwave photonic filter," *Nat. Commun.* **13**, 7798 (2022).
- ²⁰M. S. Rasras, D. M. Gill, S. S. Patel, K.-Y. Tu, Y.-K. Chen, A. E. White, A. T. S. Pomerene, D. N. Carothers, M. J. Grove, D. K. Sparacin, J. Michel, M. A. Beals, and L. C. Kimerling, "Demonstration of a fourth-order Pole-zero optical filter integrated using CMOS processes," *J. Lightwave Technol.* **25**, 87–92 (2007).
- ²¹L. Zhuang, M. Hoekman, R. M. Oldenbeuving, K.-J. Boller, and C. G. H. Roeloffzen, "CRIT-alternative narrow-passband waveguide filter for microwave photonic signal processors," *IEEE Photonics Technol. Lett.* **26**, 1034–1037 (2014).
- ²²L. Zhuang, M. Burla, C. Taddei, C. G. H. Roeloffzen, M. Hoekman, A. Leinse, K. J. Boller, and A. J. Lowery, "Integrated microwave photonic splitter with reconfigurable amplitude, phase, and delay offsets," *Opt. Lett.* **40**, 5618 (2015).
- ²³L. Zhuang, C. Zhu, Y. Xie, M. Burla, C. G. H. Roeloffzen, M. Hoekman, B. Corcoran, and A. J. Lowery, "Nyquist-filtering (De)Multiplexer using a ring resonator assisted interferometer circuit," *J. Lightwave Technol.* **34**, 1732–1738 (2016).
- ²⁴Z. Geng, Y. Xie, L. Zhuang, M. Burla, M. Hoekman, C. G. H. Roeloffzen, and A. J. Lowery, "Photonic integrated circuit implementation of a sub-GHz-selectivity frequency comb filter for optical clock multiplication," *Opt. Express* **25**, 27635 (2017).
- ²⁵Q. Sun, L. Zhou, L. Lu, G. Zhou, and J. Chen, "Reconfigurable high-resolution microwave photonic filter based on dual-ring-assisted MZIs on the Si₃N₄ platform," *IEEE Photonics J.* **10**, 1–12 (2018).
- ²⁶M. Wang, X. Chen, U. Khan, and W. Bogaerts, "Programmable wavelength filter with double ring loaded MZI," *Sci. Rep.* **12**, 1482 (2022).
- ²⁷A. Singh, R. Belansky, and M. Soltani, "Ultraflat bandpass, high extinction, and tunable silicon photonic filters," *Opt. Express* **30**, 43787 (2022).
- ²⁸C. Madsen, "Efficient architectures for exactly realizing optical filters with optimum bandpass designs," *IEEE Photonics Technol. Lett.* **10**, 1136–1138 (1998).
- ²⁹G. Choo, S. Cai, B. Wang, C. K. Madsen, K. Entesari, and S. Palermo, "Automatic monitor-based tuning of reconfigurable silicon photonic APF-based Pole/zero filters," *J. Lightwave Technol.* **36**, 1899–1911 (2018).
- ³⁰M. J. Shawon and V. Saxena, "Fully automatic in-situ reconfiguration of optical filters in a CMOS-compatible silicon photonic process," *J. Lightwave Technol.* **41**, 1286–1297 (2023).
- ³¹D. Pérez-López, A. Gutiérrez, and J. Capmany, "Silicon nitride programmable photonic processor with folded heaters," *Opt. Express* **29**, 9043 (2021).
- ³²L. Zhuang, "Flexible RF filter using a nonuniform SCISSOR," *Opt. Lett.* **41**, 1118 (2016).
- ³³C. K. Madsen and J. H. Zhao, *Optical Filter Design and Analysis: A Signal Processing Approach* (John Wiley, 1999), p. 408.
- ³⁴D. Pérez-López, A. M. Gutierrez, E. Sánchez, P. DasMahapatra, and J. Capmany, "Integrated photonic tunable basic units using dual-drive directional couplers," *Opt. Express* **27**, 38071–38086 (2019).